Chemical Science

ROYAL SOCIETY OF CHEMISTRY

EDGE ARTICLE

View Article Online
View Journal | View Issue

Cite this: *Chem. Sci.*, 2026, **17**, 6178

All publication charges for this article have been paid for by the Royal Society of Chemistry

Received 31st July 2025
Accepted 24th January 2026

DOI: 10.1039/d5sc05793k

rsc.li/chemical-science

Making room for reactivity in topochemical transformations under pressure

Tengteng Lyu,†[a] Jonathan B. Lefton,†[b] Martin Etter,[c] Shrikant Bhat,[c] Wenhao Liu,[d] Bing Lv,[d] Luke J. Kwan,[b] Hao Yan*[a] and Tomče Runčevski*[b]

The orderly arrangement of molecules in crystals provides a unique platform for the control of reactivity, where spatial vicinity and orientation of the molecules determine the course of the reaction. Common wisdom assumes that the densest crystal packings of the reactant molecules are most favorable for pressure-induced topochemical reactions. Based on thermodynamic and spatial arguments, here we show that the densest crystal packing may not be the most optimal platform for chemical synthesis. Instead, introducing void space within the crystal lattice significantly improves and even enables chemical reactions. In the case of sorbic acid confined between brucite-type layers, this reactivity is used to modify the optical, spectroscopic and magnetic properties of 2D layers and to synthesize a retrievable polymeric product.

Introduction

In topochemical reactions the spatial arrangement of molecules within a crystal lattice dictates the reaction pathway.[1] These reactions have emerged as synthetic routes towards polymers with unprecedented regio- and stereoselectivity[2–20] and as a means to control the physical properties of the crystal.[21–35] Light, heat, and pressure are common stimuli, and densely packed structures, where reactants are in closest proximity, are intuitively regarded as the most favorable platforms for chemical reactivity. Based on fundamental thermodynamic considerations, we hypothesize that, perhaps contra-intuitively, providing ample space within the crystal packing can lower the energy barriers for pressure-induced transformations, hinder reversible reactions upon decompression, and enable permanent change in the physical properties of the crystal and retrievable polymeric product.

Derived from the fundamental equation for internal energy, the pressure-induced energization of solids is governed by

$$\left(\frac{\partial U}{\partial p}\right)_T \approx \beta p V$$

where $\beta = -\frac{1}{V}\left(\frac{\partial V}{\partial p}\right)_T$ is the isothermal compressibility. From this equation, it follows that $\left(\frac{\partial U}{\partial p}\right)_T$ increases with β, and thus the energization effect of pressure is greater on systems with larger compressibility. Compression also decreases the system's entropy, that is, $\left(\frac{\partial S}{\partial p}\right)_T = -\left(\frac{\partial V}{\partial T}\right)_p < 0$, further driving the reaction forward. In solid-state reaction systems, this is manifested as reduced conformational space of the reactant, leading to enhanced selectivity. In fact, the simultaneous increase in energy and selectivity in pressure-driven systems is distinct from thermally driven systems, where heat increases both the energy and entropy, generally leading to decreased selectivity. Finally, a large volumetric reduction thermodynamically favors pressure-driven reactions, based on the fundamental equation for the Gibbs energy:

$$\left(\frac{\partial \Delta_r G}{\partial p}\right)_T = \Delta_r V$$

where a large and negative $\Delta_r V$ corresponds to a negative reaction Gibbs energy ($\Delta_r G$) and spontaneity.

Based on these thermodynamic considerations, it follows that large β and large and negative $\Delta_r V$ contribute to lowering the energy barriers and facilitating, even enabling, topochemical reactions. Consequently, instead of densely packed structures, packings capable of undergoing large volume changes emerge as favorable platforms for topochemical reactivity. Ample space within the crystal packing also facilitates reactivity due to spatial considerations. For example, topochemical polymerizations of unsaturated hydrocarbons change the carbon atom hybridization (sp/sp^2 to sp^2/sp^3), which requires structural reorganization that can be more easily accommodated in packings with larger free volume around the reactive centers.

[a]*Department of Chemistry, University of North Texas, Denton, Texas 76205, USA. E-mail: hao.yan@unt.edu*

[b]*Department of Chemistry, Southern Methodist University, Dallas, TX 75275, USA. E-mail: truncevski@smu.edu*

[c]*Deutsche Elektronen-Synchrotron DESY, Notkestrasse 85, 22607 Hamburg, Germany*

[d]*Department of Physics, University of Texas at Dallas, Richardson, TX 75080, USA*

† These authors contributed equally.

Experimental realization of ordered structures with larger free volume is challenging, as molecules have a natural tendency to adopt the densest crystal packing. However, there are viable strategies to achieve lower packing density.[36–49] For example, carboxylic acids can be grafted onto brucite-type layers replacing hydroxide anions.[50,51] The spacing between molecules in such hybrids is, to a large extent, controlled by the spacing between the metal ions in the robust inorganic layer, and it can often lead to a decrease in the packing density of the carboxylate anions. Furthermore, in a subset of these structures, only half of the hydroxides get replaced leading to a substantial amount of added space. We have shown that sorbic acid replaces half of the OH^- anions in brucite-type $Co(OH)_2$, forming Co(OH)(sorb) (Fig. 1a).[52] Considering that OH^- occupies significantly less space than sorbate anions, the interlayer in Co(OH)(sorb) has lower local crystal density compared to layered structures containing only sorbate anions, such as $Mn(sorb)_2$ (Fig. 1b). The markedly different crystal density of their interlayers, with additional ample space caused by the presence of OH^- in Co(OH)(sorb), presents an ideal opportunity to test the thermodynamic and spatial considerations for adding ample volume in pressure-induced reactions in order to enable chemical reactivity (Fig. 1c).

Results and discussion

First, we tested the pressure-induced reactivity of Co(OH)(sorb). Synchrotron X-ray powder diffraction (XRPD) patterns collected as a function of pressure (Fig. S1) show 2θ shift to higher angles, indicating compression of the lattice. Fig. 2a shows the response of the (001) peak to pressure corresponding to the inter-layer distance (Fig. S2). The lattice spacing, d_{001}, decreases by 1.8 Å from ambient pressure to 10 GPa (Fig. 2b), reflecting the compression of the interlayer occupied by sorbates. Notably, the (001) peak shifts slightly to the left from 10.5 to 13.5 GPa, indicating a negative linear compressibility in this pressure range and suggesting non-mechanical effects. Upon decompression, the d_{001} distance shows an irreversible decrease, with a hysteresis in the d_{001} distance–pressure plot. This observation indicates an irreversible change in the organic interlayer. *In situ* compression of the sample led to a reduction in crystallinity, particularly evident from the diminishing intensity of the high-angle reflections, which prevented detailed structural analysis. Powder diffraction data collected after decompression confirmed an irreversible loss of crystallinity.

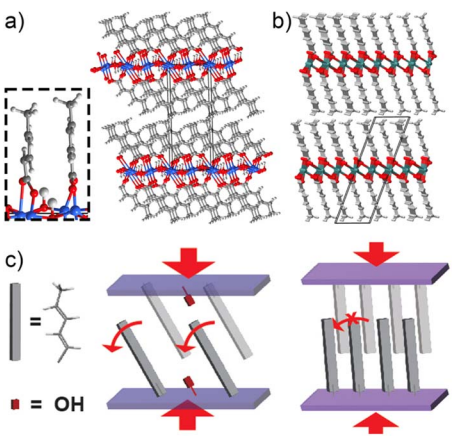

Fig. 1 Crystal packing of (a) Co(OH)(sorb) and (b) $Mn(sorb)_2$. (c) Schematic representation of pressure-induced reactivity. (Oxygen: red, carbon: gray, hydrogen: off-white, cobalt: blue, and manganese: green).

Optical spectra of the compressed sample (Fig. 2c) show the emergence of absorption at 550 nm, resulting in a color change from orange to purple (Fig. 2d). These experimental observations indicate irreversible changes in the local environment of the Co^{2+} cations, caused by changes in the interlayer.

In situ Raman spectra (Fig. 2e) reveal an increase in the full-width-at-half-maximum (FWHM) of the C=C stretching modes[53] at ~1656 cm^{-1} during compression (Fig. 2f). The increase in FWHM is prominent and abrupt around 10 GPa, indicating major changes in the structure and environment of the C=C stretching modes. Density-functional theory (DFT) simulations confirmed that the number of non-degenerate normal modes associated with C=C stretching increases with the degree of oligomerization (Fig. S3). We attribute this broadening to chemical reactivity and the formation of extended molecules in the organic interlayer. The polymerization likely initiates simultaneously at multiple sites and propagates at variable rates, resulting in randomly distributed domains with variable chain lengths. The disruption of in-plane order may also contribute to the broadening of the Raman peaks. The broadening persists after decompression indicating that the polymeric product can be retrieved.

In the low-frequency region of the Raman spectrum (Fig. 2g), three peaks at 30, 80 and 110 cm^{-1} are present at ambient pressure, corresponding to lattice vibrations in ordered 2D materials.[54] These peaks vanish at 8.4 GPa and are not recovered upon releasing the pressure.

Our previous studies have shown that anisotropic deformation is key to reactivity under isotropic compression.[55,56] In Co(OH)(sorb), the structure is bound by van der Waals interactions in the (001) direction, making it more compressible than the in-plane directions bound by ionic and/or coordination bonds. This environment, together with the presence of reactive unsaturated carbon atoms in close proximity, leads to pressure-induced polymerization. The structural and chemical changes were explained using density functional theory (DFT) calculations (Fig. 3a). Theoretical modeling shows irreversible reduction of both the d_{001} and the unit cell volume upon compression (Fig. 3b, S4 and S5), consistent with the experimental XPRD data (Fig. 2a). The unit cell contraction is anisotropic, with a larger decrease in the (001) direction than in the other axes, leading to a large contraction of the interlayer spacing. The presence of OH^- groups in the Co–O inorganic plane creates gaps between the adjacent sorbates, thereby sterically allowing for tilting motion of the sorbates (Fig. 3c), bringing the reactive atoms closer together (Fig. 3d) and allowing for an overlap of frontier orbitals (Fig. 3e). This environment eventually leads to chemical reactivity and formation of a polymer (Fig. 3f). The calculated bond formation pressure, 35 GPa, is higher than the experimental value (~10 GPa), due to

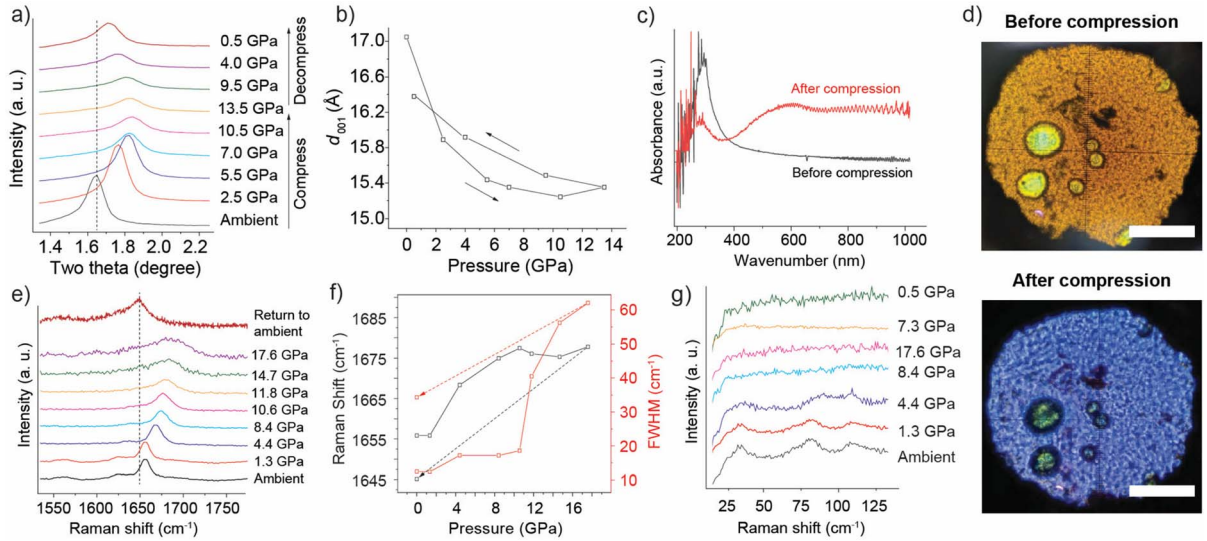

Fig. 2 (a) Synchrotron XRD patterns (wavelength: 0.496 Å) and (b) d_{001} *versus* pressure for Co(OH)(sorb). (c) Optical spectra and (d) photographs before and after compression (bar = 50 μm). (e) Raman spectra in the C=C stretching region and (f) Raman shift and full width at half maximum (FWHM) for Co(OH)(sorb). (g) Low-frequency Raman spectra.

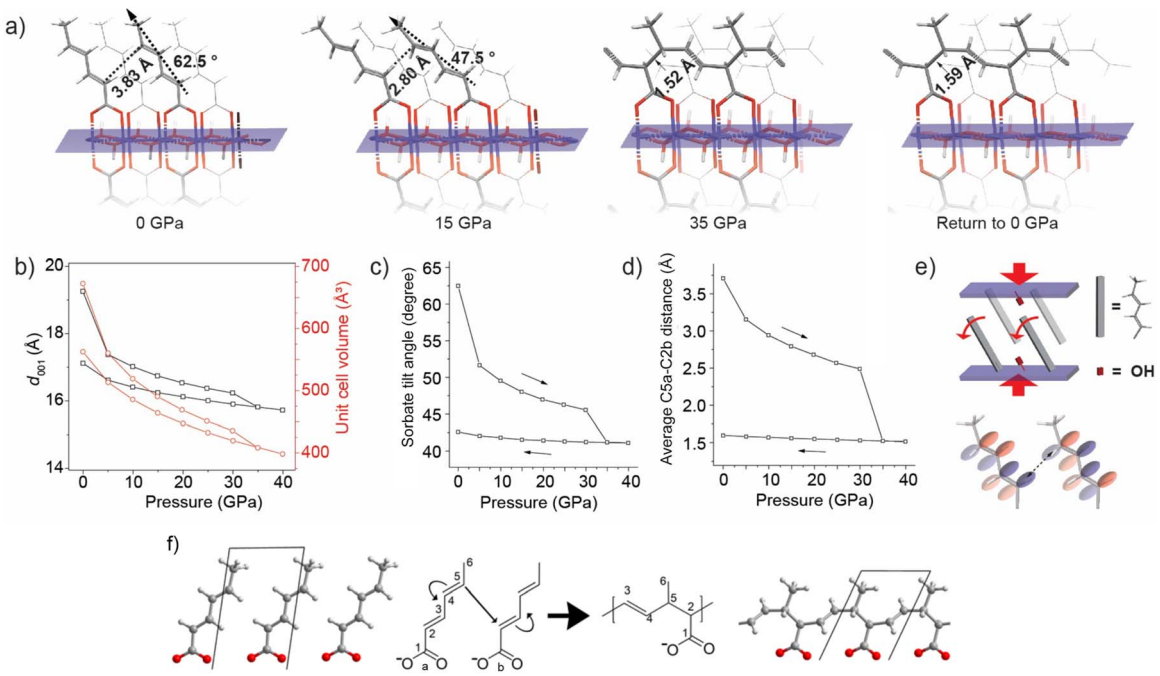

Fig. 3 (a) DFT simulated Co(OH)(sorb) structures at 0, 15, and 35 and back to 0 GPa. Blue, red, grey and white represent Co, O, C and H, respectively. (b) Unit cell volume and d_{001}. (c) Sorbate tilting angle. (d) Average C5a–C2b distance as a function of pressure. (e) Schematic reaction mechanism. (f) Polymeric structure of the product.

multiple factors including the omission of thermal fluctuations and limited phase space searched by the local optimization algorithm. We note that the DFT results do not capture the experimentally observed negative compressibility of d_{001} from XRPD measurements, likely due to limitations in the description of dispersive forces that dominate interlayer interactions.

To retrieve macroscopic amounts of the product, we used a six-ram Hall-type large volume press. The compressed product, HP-Co(OH)(sorb), had purple color (Fig. S6), consistent with optical spectroscopy measurements (Fig. 2c and d). This observation confirms that this topochemical reaction can be scaled-up and the product can be successfully retrieved.

Part of the sample was dissolved in a $DCl/D_2O/CD_3OD$ solvent, suitable for measuring nuclear magnetic resonance (NMR) spectra. The dissolution resulted in the release of the Co^{2+} and OH^- ions and unreacted sorbates, leaving an

insoluble, swollen, white colored organic material (Fig. S7). We note that pristine, unreacted Co(OH)(sorb) is soluble in the solvent and does not leave a residue. This outcome is expected for the presence of an organic polymer in the interlayer. Proton nuclear magnetic resonance (^{1}H NMR) spectra of HP-Co(OH)(sorb) show new peaks at 0.97 and 1.67 ppm (Fig. S8), indicative of hydrogen atoms bonded to sp^3-hybridized carbon, as observed in the theoretical calculations (Fig. 3). Simulation of the ^{1}H NMR spectra of oligomeric products (Fig. S9) further confirms the occurrence of irreversible, pressure-induced chemical reactions in the organic interlayer.

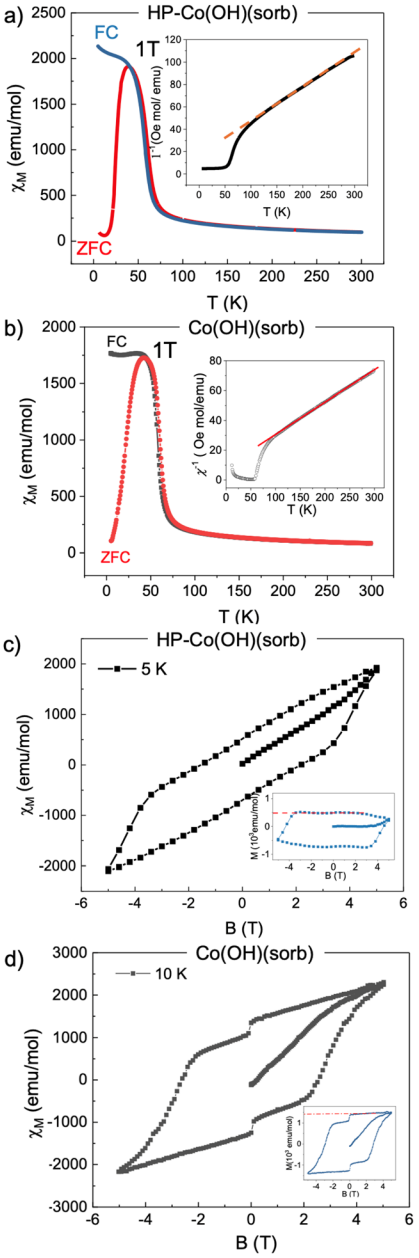

Fig. 4 Temperature dependent magnetic susceptibility data of (a) HP-Co(OH)(sorb) and (b) Co(OH)(sorb). The insets in (a) and (b) show inverse magnetization, and the red dashed line indicates Curie Weiss fitting. Magnetization hysteresis of (c) HP-Co(OH)(sorb) and (d) Co(OH)(sorb).

The diffraction and spectroscopic observation indicate irreversible changes and potential disorder in the 2D layer caused by the chemical reaction in the interlayer. It follows that structural changes in the organic structure can be used as a direct strategy to modify the properties of the inorganic layers. One notable physical property of the brucite-type 2D layers in Co(OH)(sorb) is their magnetic behavior, as we have previously shown that the material exhibits canted antiferromagnetism.[52]

The temperature dependent magnetic susceptibility of HP-Co(OH)(sorb) initially shows paramagnetic behavior upon cooling (Fig. 4a), followed by a sudden decrease of magnetization, similar to Co(OH)(sorb) (Fig. 4b). The zero-field-cooled (ZFC) data indicate that the antiferromagnetic Néel temperature occurs at T_N = 38 K (3.7 K lower than T_N = 41.7 K for Co(OH)(sorb)). The material shows bifurcation between the ZFC and field-cooled data, confirming that there are net ferromagnetic moments arising from canted antiferromagnetic (AFM) states. The susceptibility follows the Curie Weiss law $\chi = C/(T - \Theta)$ quite nicely (Fig. 4a), with a $\theta_{CW} = -17$ K (similar to $\theta_{CW} = -20$ K for Co(OH)(sorb)). The negative θ_{CW} further confirms antiferromagnetic coupling. The effective magnetic moment, μ_{eff}, calculated from the Curie constant is 4.49 μ_B/Co^{II} for HP-Co(OH)(sorb). In contrast, for Co(OH)(sorb), μ_{eff} is estimated to be 3.79 μ_{eff}/Co^{II}, which is very close to the value of free Co(II) ions of 3.87 μ_{eff}/Co^{II}.

$$C = \frac{\mu_0 {\mu_{eff}}^2}{3k_B}$$

The field dependence measurements of the magnetization from −5 to 5T were carried out to further explore the nature of magnetic order of the material before and after high pressure treatment. The magnetization of HP-Co(OH)(sorb) does not saturate at high magnetic fields but instead shows a quasi-linear relation with the external magnetic field, H (Fig. 4c). Similar behavior was observed for Co(OH)(sorb) (Fig. 4d). The linear relation of M–H and the existence of magnetic hysteresis further indicate canted antiferromagnetism of the sample. To extract the saturation moment from the net ferromagnetism where the ferromagnetic order is provided by the small component canted by the magnetic moment of Co, the M–H curves were fitted using

$$M(H) = M_s + M_{AFM}.$$

For HP-Co(OH)(sorb), the saturation field is estimated to be 0.004 μ_B/Co^{II}, smaller than 0.13 μ_B/Co^{II} in Co(OH)(sorb). All the saturation magnetic moments of the samples before and after high pressure treatment are much smaller than the effective moment estimated from the Curie–Weiss law, further indicating the scenario of canted AFM in Co(OH)(sorb). Moreover, after high pressure treatment, the saturation moment is reduced, which can be attributed to a pressure modified canting angle, resulting in diminished net ferromagnetism.

The sample before and after applying pressure shows canted antiferromagnetism and overall similar magnetic properties,

which can be attributed to the retainment of the layered structure after decompression. However, the irreversible chemical changes in the organic intralayer affect the electronic structure and local geometry of Co^{2+} cations, thus modifying the magnetic properties, evidenced in a larger effective magnetic moment, reduction of the saturation field and modification of the Néel temperature.

It has been reported that compressing crystals of sorbic acid (H(sorb))[57] does not lead to reactivity. However, the crystal packing of H(sorb) is markedly different from that of Co(OH)(sorb) and direct comparison cannot be easily drawn. Instead, as a control study, we studied the high-pressure behavior of $Mn(sorb)_2$. A hydrothermal reaction of 1 : 2 ratio of Mn^{2+} and $sorb^-$ provided yellow crystalline powder, whose structure was solved *ab initio* from high-resolution PXRD data (Fig. S10). The crystal structure features densely packed layers of sorbates, packed between inorganic Mn–O layers (Fig. 1b). The *in situ* Raman spectra show fully recovered C=C stretching mode after compression (Fig. 5a), indicating the absence of irreversible, pressure-driven polymerization. The low-frequency vibrational modes are recovered after release of pressure (Fig. 5b), further supporting their structural inertness under pressure. These modes are initially found at 34 and 50 cm^{-1} and become red-shifted to 31 and 48 cm^{-1} after recovery, suggesting only subtle structural changes.

High-pressure synchrotron XRPD further confirms the inertness of $Mn(sorb)_2$. The (100) reflection shifts from 2θ of 1.51° at ambient pressure to 1.63° at 15.9 GPa (Fig. 5d and S11), corresponding to 1.5 Å contraction of d_{100} and showing lower compressibility than Co(OH)(sorb). No apparent hysteresis is observed in the distance–pressure plot (Fig. 5e). The sample pressure remained at 0.9 GPa after fully releasing the external pressure due to remnant stress, and d_{100} arrives at 18.1 Å, slightly lower than the initial value.

DFT studies of the high-pressure structures of $Mn(sorb)_2$ (Fig. 5f) show that d_{100} and the unit cell volume decrease by 4 Å and 175 $Å^3$, respectively, from 0 to 40 GPa (Fig. 5g). Closely packed sorbates sterically hinder the tilting motion: the tilt angle decreases by 13.4° from 0 to 40 GPa (Fig. 5h) (*cf.* 21.4° in Co(OH)(sorb) in the same pressure range). The distance between the reactive carbons monotonously decreases (Fig. 5j) without indication of chemical reactivity. The absence of irreversible changes in the simulation is consistent with the experimental findings (Fig. 5a–e).

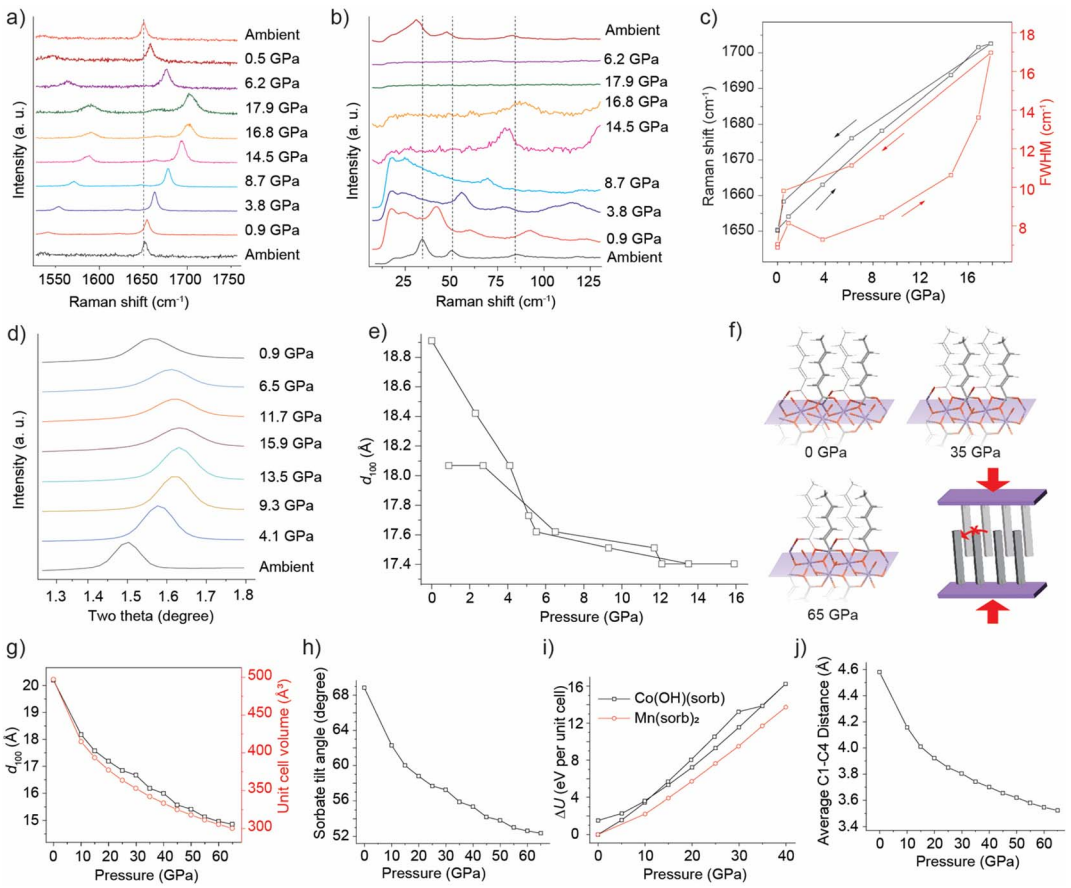

Fig. 5 Raman spectra in (a) the C=C stretching region and (b) low frequency for $Mn(sorb)_2$. (c) Raman shift and full width at half maximum (FWHM). (d) XRPD showing the (100) diffraction peak (wavelength: 0.496 Å). (e) d_{100} *versus* pressure. (f) DFT-simulated structures of $Mn(sorb)_2$ from ambient pressure to 65 GPa. The rightmost panel shows the schematic strain in the crystal. (g) d_{100} and unit cell volume *versus* pressure. (h) Sorbate tilting *versus* pressure. (i) Changes of total energy (ΔU) *versus* pressure for Co(OH)(sorb) and $Mn(sorb)_2$. (j) Average C1–C4 distance *versus* pressure upon compression.

Finally, we calculated the pressure-induced change of total energy per unit cell, ΔU, for both structures (Fig. 5i). ΔU was found to be 2.5 eV lower in $Mn(sorb)_2$ than Co(OH)(sorb) in the same pressure range, from 0 to 40 GPa. This finding is consistent with our analysis that $\left(\frac{\partial U}{\partial p}\right)_T$ depends positively on compressibility. The experimental data (Fig. 2 and 5) and the DFT calculated changes of the unit cell parameters for both systems (Fig. S4 and S5) show that the Co(OH)(sorb) system exhibits hysteresis compared to $Mn(sorb)_2$ with respect to lattice parameters, beta angle and total energy during compression and decompression, indicative of irreversible chemical reactivity enabled by the introduced void space within the crystal lattice.

Additionally, it is worth mentioning that sorbic acid crystals are not readily polymerizable by light or heat.[58–60] The same holds true for salts such as Co(OH)(sorb) and $Mn(sorb)_2$. Prolonged UV-irradiation of both salts did not lead to formation of the product.

Conclusions

In summary, the topochemical reaction in Co(OH)(sorb) together with the absence of chemical reactivity in $Mn(sorb)_2$ and H(sorb) indicates that additional free volume between sorbates facilitates reactivity and stabilization of the product. This rather counter-intuitive conclusion is supported by thermodynamic and spatial considerations. Larger free volume leads to a large isothermal compressibility which increases pressure-induced energization and enables the reactant to overcome the activation barriers. Reducing the free volume following the chemical reaction leads to a negative reaction volume corresponding to a negative reaction Gibbs energy and driving the reaction forward. Finally, the presence of voids allows for conformational reorganization required by changes in hybridization.

While further studies are necessary to generalize these conclusions, this design strategy is a valuable new addition to the solid-state chemistry toolbox. It is applicable to a wide range of systems prone to engineering added void space. These include 2D hybrids,[49–51,61] hydrogen-bonded,[36,37,46] metal–organic[38,48] and covalent organic[39] frameworks, molecular cages,[40,41,62] porous crystals,[42–45] and other classes of materials. This approach facilitates or even enables reactivity that can be used to fine-tune the physical properties of the crystal, and it allows for the synthesis of atomically precise polymers with unprecedented stereoselectivity. Further developments and generalization of this design strategy can open exciting new directions in crystal chemistry.

Author contributions

Conceptualization: TR and HY. Formal analysis and investigation: TL, JBL, ME, SB, WL, BL, LJK, HY, and TR. Funding acquisition: TR and BL. Project administration: TR and HY. Supervision: TR, HY, and BL. Writing – original draft: TR and HY. Writing – review & editing: TL, JBL, ME, SB, WL, BL, LJK, HY, and TR.

Conflicts of interest

There are no conflicts to declare.

Data availability

The data supporting this article have been included as part of the supplementary information (SI) or data is available by request. Supplementary information: includes material preparation and, experimental procedures, computational and crystallographic details, images and spctroscopic data. CCDC 2526627 contains supplementary crystallographic data for this paper.[63] See DOI: https://doi.org/10.1039/d5sc05793k.

Acknowledgements

This material is partly based upon work supported by the National Science Foundation under grant no. DMR-2143581. We acknowledge DESY (Hamburg, Germany), a member of the Helmholtz Association HGF, for the provision of experimental facilities. Parts of this research were carried out at PETRA III beamlines P02.1 and P61B. Beamtime was allocated by an in-house contingent. TR acknowledges DESY's Stephenson Distinguished Visitor Programme. The work at UT Dallas was supported by US Air Force Office of Scientific Research grant no. FA9550-19-1-0037, National Science Foundation-DMREF-2324033, and Office of Naval Research grant no. N00014-23-1-2020 and N00014-22-1-2755. This research used resources of the Advanced Light Source, a U.S. DOE Office of Science User Facility under contract no. DE-AC02-05CH11231. This work used CRUNTCH, the high-performance computational facility at University of North Texas supported by the National Science Foundation under grant no, CHE-1531468 and OAC-2117247.

Notes and references

1 G. M. J. Schmidt, Photodimerization in the Solid State, *Pure Appl. Chem.*, 1971, **27**(4), 647–678, DOI: 10.1351/pac197127040647.
2 J. W. Colson and W. R. Dichtel, Rationally Synthesized Two-Dimensional Polymers, *Nat. Chem.*, 2013, **5**(6), 453–465, DOI: 10.1038/nchem.1628.
3 K. Hema, A. Ravi, C. Raju, J. R. Pathan, R. Rai and K. M. Sureshan, Topochemical Polymerizations for the Solid-State Synthesis of Organic Polymers, *Chem. Soc. Rev.*, 2021, **50**(6), 4062–4099, DOI: 10.1039/D0CS00840K.
4 J. W. Lauher, F. W. Fowler and N. S. Goroff, Single-Crystal-to-Single-Crystal Topochemical Polymerizations by Design, *Acc. Chem. Res.*, 2008, **41**(9), 1215–1229, DOI: 10.1021/ar8001427.
5 R. Mohanrao, K. Hema and K. M. Sureshan, Topochemical Synthesis of Different Polymorphs of Polymers as a Paradigm for Tuning Properties of Polymers, *Nat. Commun.*, 2020, **11**(1), 865, DOI: 10.1038/s41467-020-14733-y.

6 H. Balan and K. M. Sureshan, Hierarchical Single-Crystal-to-Single-Crystal Transformations of a Monomer to a 1D-Polymer and Then to a 2D-Polymer, *Nat. Commun.*, 2024, **15**(1), 6638, DOI: 10.1038/s41467-024-51051-z.

7 M. Murphy, A. Mohamed, J. V. Badding and E. Elacqua, Rational Approaches toward the Design and Synthesis of Carbon Nanothreads, *Acc. Chem. Res.*, 2025, 5c00172, DOI: 10.1021/acs.accounts.5c00172.

8 S. Huss, S. Wu, B. Chen, T. Wang, M. C. Gerthoffer, D. J. Ryan, S. E. Smith, V. H. Crespi, J. V. Badding and E. Elacqua, Scalable Synthesis of Crystalline One-Dimensional Carbon Nanothreads through Modest-Pressure Polymerization of Furan, *ACS Nano*, 2021, **15**(3), 4134–4143, DOI: 10.1021/acsnano.0c10400.

9 W. Zhao, J. Zhang, Z. Sun, G. Xiao, H. Zheng, K. Li, M.-R. Li and B. Zou, Chemical Synthesis Driven by High Pressure, *CCS Chem.*, 2025, **7**(5), 1250–1271, DOI: 10.31635/ccschem.024.202405293.

10 K. Hema, A. Ravi, C. Raju and K. M. Sureshan, Polymers with Advanced Structural and Supramolecular Features Synthesized through Topochemical Polymerization, *Chem. Sci.*, 2021, **12**(15), 5361–5380, DOI: 10.1039/d0sc07066a.

11 R. Khazeber and K. M. Sureshan, Topochemical Ene–Azide Cycloaddition Reaction, *Angew. Chem.*, 2021, **133**(47), 25079–25085, DOI: 10.1002/ange.202109344.

12 R. Singh, A. Siddharthan and K. M. Sureshan, Topochemical Alkyne Nitrile Oxide Cycloaddition for Polymer Synthesis, *Angew. Chem., Int. Ed.*, 2025, **64**(52), e20947, DOI: 10.1002/anie.202520947.

13 A. Calderón-Díaz, L. Ordner, M. G. Bernbeck, M. Palesati, M. Weber, N. Stingelin and W. R. Gutekunst, Topochemical Ring-Opening Polymerization of an Oxathianethione, *J. Am. Chem. Soc.*, 2025, **147**(25), 21331–21338, DOI: 10.1021/jacs.5c06180.

14 S. Pathak and K. M. Sureshan, A Syndiotactic Polymer via Spontaneous Exoselective Single-Crystal-To-Single-Crystal Topochemical Diels–Alder Cycloaddition Reaction, *J. Am. Chem. Soc.*, 2024, **146**(44), 30495–30501, DOI: 10.1021/jacs.4c11426.

15 A. Lal, M. C. Madhusudhanan and K. M. Sureshan, Large Molecular Rotation in Crystal Changes the Course of a Topochemical Diels–Alder Reaction from a Predicted Polymerization to an Unexpected Intramolecular Cyclization, *Angew. Chem.*, 2024, **136**(43), e202411165, DOI: 10.1002/ange.202411165.

16 Z. Wang, Y. Pei, A. Hao and P. Xing, Topochemical Synthesis of Chiroptical Materials through Charge-Transfer/Diels–Alder Cascade Reaction, *Nat. Commun.*, 2025, **16**(1), 5539, DOI: 10.1038/s41467-025-60790-6.

17 M. C. Gerthoffer, S. Wu, B. Chen, T. Wang, S. Huss, S. M. Oburn, V. H. Crespi, J. V. Badding and E. Elacqua, 'Sacrificial' Supramolecular Assembly and Pressure-Induced Polymerization: Toward Sequence-Defined Functionalized Nanothreads, *Chem. Sci.*, 2020, **11**(42), 11419–11424, DOI: 10.1039/D0SC03904G.

18 S. K. Gupta, R. Khazeber, K. S. Siddharth, A. Balakrishnan and K. M. Sureshan, Topochemical Synthesis of a Syndiotactic Polymer from a Racemic Monomer, *J. Am. Chem. Soc.*, 2025, **147**(49), 45731–45739, DOI: 10.1021/jacs.5c18292.

19 H. Balan, S. Shahanas and K. M. Sureshan, Single-Crystal-to-Single-Crystal Synthesis of an Adaptive Two-Dimensional Polymer with Dynamic Pores, *J. Am. Chem. Soc.*, 2025, **147**(41), 37798–37807, DOI: 10.1021/jacs.5c13942.

20 A. Lal and K. M. Sureshan, Isomer-Dependent Reactivity in the Solid State: Topochemical [4 + 4] *vs.* [4 + 2] Cycloaddition Reactions, *Chem. Sci.*, 2025, **16**(29), 13496–13502, DOI: 10.1039/D5SC02327K.

21 P. Naumov, S. Chizhik, M. K. Panda, N. K. Nath and E. Boldyreva, Mechanically Responsive Molecular Crystals, *Chem. Rev.*, 2015, **115**(22), 12440–12490, DOI: 10.1021/acs.chemrev.5b00398.

22 A. Nyayachavadi, A. K. Sur, P. Kulatunga, Y. Wang, T. C. Gomes, M. Mooney, G. T. Mason, A. Hu, X. Gu and S. Rondeau-Gagné, Covalent Topochemical Photo-Cross-Linking of Diketopyrrolopyrrole-Based Polymers with Polydiacetylenes toward Tunable Mechanical and Electronic Properties, *Chem. Mater.*, 2023, **35**(22), 9682–9691, DOI: 10.1021/acs.chemmater.3c02025.

23 Z. Wei, X. Wang, B. Seo, X. Luo, Q. Hu, J. Jones, M. Zeller, K. Wang, B. M. Savoie, K. Zhao and L. Dou, Side-Chain Control of Topochemical Polymer Single Crystals with Tunable Elastic Modulus, *Angew. Chem., Int. Ed.*, 2022, **61**(49), e202213840, DOI: 10.1002/anie.202213840.

24 K. Wissel, A. M. Malik, S. Vasala, S. Plana-Ruiz, U. Kolb, P. R. Slater, I. Da Silva, L. Alff, J. Rohrer and O. Clemens, Topochemical Reduction of La_2 NiO_3 F_2 : The First Ni-Based Ruddlesden–Popper $n = 1$ T′-Type Structure and the Impact of Reduction on Magnetic Ordering, *Chem. Mater.*, 2020, **32**(7), 3160–3179, DOI: 10.1021/acs.chemmater.0c00193.

25 L. M. Wheeler, T. L. Phan, M. A. Smeaton, S. Acharya, S. Hariyani, M. E. Alexander, M. I. Gonzalez, E. M. Miller, D. W. Mulder, S. Banerjee, K. L. Jungjohann, A. J. Ferguson and J. L. Blackburn, Tuning Optical and Electrical Properties of Vanadium Oxide with Topochemical Reduction and Substitutional Tin, *Chem. Mater.*, 2024, **36**(21), 10483–10495, DOI: 10.1021/acs.chemmater.4c01557.

26 L. R. MacGillivray, G. S. Papaefstathiou, T. Friščić, T. D. Hamilton, D.-K. Bučar, Q. Chu, D. B. Varshney and I. G. Georgiev, Supramolecular Control of Reactivity in the Solid State: From Templates to Ladderanes to Metal–Organic Frameworks, *Acc. Chem. Res.*, 2008, **41**(2), 280–291, DOI: 10.1021/ar700145r.

27 R. Medishetty, A. Husain, Z. Bai, T. Runčevski, R. E. Dinnebier, P. Naumov and J. J. Vittal, Single Crystals Popping Under UV Light: A Photosalient Effect Triggered by a [2+2] Cycloaddition Reaction, *Angew. Chem.*, 2014, **126**(23), 6017–6021, DOI: 10.1002/ange.201402040.

28 M. K. Panda, T. Runčevski, A. Husain, R. E. Dinnebier and P. Naumov, Perpetually Self-Propelling Chiral Single Crystals, *J. Am. Chem. Soc.*, 2015, **137**(5), 1895–1902, DOI: 10.1021/ja5111927.

29 R. Rai, B. P. Krishnan and K. M. Sureshan, Chirality-Controlled Spontaneous Twisting of Crystals Due to Thermal Topochemical Reaction, *Proc. Natl. Acad. Sci. U. S. A.*, 2018, **115**(12), 2896–2901, DOI: 10.1073/pnas.1718965115.

30 S. Yamanaka, N. S. Kini, A. Kubo, S. Jida and H. Kuramoto, Topochemical 3D Polymerization of C_{60} under High Pressure at Elevated Temperatures, *J. Am. Chem. Soc.*, 2008, **130**(13), 4303–4309, DOI: 10.1021/ja076761k.

31 X. Feng, K. Bu, T. Liu, S. Guo, Z. Sun, T. Fu, Y. Xu, K. Liu, S. Yang, Y. Zhao, H. Li, X. Lü and T. Zhai, Giant Tunability of Charge Transport in 2D Inorganic Molecular Crystals by Pressure Engineering, *Angew. Chem.*, 2023, **135**(9), e202217238, DOI: 10.1002/ange.202217238.

32 S. G. Duyker, G. J. Halder, P. D. Southon, D. J. Price, A. J. Edwards, V. K. Peterson and C. J. Kepert, Topotactic Structural Conversion and Hydration-Dependent Thermal Expansion in Robust $LnM^{III}(CN)_6 \cdot nH_2O$ and Flexible $ALnFe^{II}(CN)_6 \cdot nH_2O$ Frameworks (A = Li, Na, K; Ln = La–Lu, Y; M = Co, Fe; $0 \leq n \leq 5$), *Chem. Sci.*, 2014, **5**(9), 3409, DOI: 10.1039/c4sc00809j.

33 G. Aromí, C. M. Beavers, J. Sánchez Costa, G. A. Craig, G. Mínguez Espallargas, A. Orera and O. Roubeau, Snapshots of a Solid-State Transformation: Coexistence of Three Phases Trapped in One Crystal, *Chem. Sci.*, 2016, **7**(4), 2907–2915, DOI: 10.1039/c5sc04287a.

34 A. Jaffe, Y. Lin, C. M. Beavers, J. Voss, W. L. Mao and H. I. Karunadasa, High-Pressure Single-Crystal Structures of 3D Lead-Halide Hybrid Perovskites and Pressure Effects on Their Electronic and Optical Properties, *ACS Cent. Sci.*, 2016, **2**(4), 201–209, DOI: 10.1021/acscentsci.6b00055.

35 A. Jaffe, Y. Lin, W. L. Mao and H. I. Karunadasa, Pressure-Induced Conductivity and Yellow-to-Black Piezochromism in a Layered Cu–Cl Hybrid Perovskite, *J. Am. Chem. Soc.*, 2015, **137**(4), 1673–1678, DOI: 10.1021/ja512396m.

36 R.-B. Lin, Y. He, P. Li, H. Wang, W. Zhou and B. Chen, Multifunctional Porous Hydrogen-Bonded Organic Framework Materials, *Chem. Soc. Rev.*, 2019, **48**(5), 1362–1389, DOI: 10.1039/C8CS00155C.

37 V. A. Russell, M. C. Etter and M. D. Ward, Layered Materials by Molecular Design: Structural Enforcement by Hydrogen Bonding in Guanidinium Alkane- and Arenesulfonates, *J. Am. Chem. Soc.*, 1994, **116**(5), 1941–1952, DOI: 10.1021/ja00084a039.

38 H.-C. Zhou, J. R. Long and O. M. Yaghi, Introduction to Metal–Organic Frameworks, *Chem. Rev.*, 2012, **112**(2), 673–674, DOI: 10.1021/cr300014x.

39 X. Feng, X. Ding and D. Jiang, Covalent Organic Frameworks, *Chem. Soc. Rev.*, 2012, **41**(18), 6010, DOI: 10.1039/c2cs35157a.

40 X. Yang, Z. Ullah, J. F. Stoddart and C. T. Yavuz, Porous Organic Cages, *Chem. Rev.*, 2023, **123**(8), 4602–4634, DOI: 10.1021/acs.chemrev.2c00667.

41 A. J. Gosselin, A. M. Antonio, K. J. Korman, M. M. Deegan, G. P. A. Yap and E. D. Bloch, Elaboration of Porous Salts, *J. Am. Chem. Soc.*, 2021, **143**(37), 14956–14961, DOI: 10.1021/jacs.1c05613.

42 J. R. Holst, A. Trewin and A. I. Cooper, Porous Organic Molecules, *Nat. Chem.*, 2010, **2**(11), 915–920, DOI: 10.1038/nchem.873.

43 S. Horike, S. Shimomura and S. Kitagawa, Soft Porous Crystals, *Nat. Chem.*, 2009, **1**(9), 695–704, DOI: 10.1038/nchem.444.

44 T.-H. Chen, I. Popov, W. Kaveevivitchai, Y.-C. Chuang, Y.-S. Chen, O. Daugulis, A. J. Jacobson and O. Š. Miljanić, Thermally Robust and Porous Noncovalent Organic Framework with High Affinity for Fluorocarbons and CFCs, *Nat. Commun.*, 2014, **5**(1), 5131, DOI: 10.1038/ncomms6131.

45 C. M. Kane, O. Ugono, L. J. Barbour and K. T. Holman, Many Simple Molecular Cavitands Are Intrinsically Porous (Zero-Dimensional Pore) Materials, *Chem. Mater.*, 2015, **27**(21), 7337–7354, DOI: 10.1021/acs.chemmater.5b02972.

46 C. B. Aakeröy and K. R. Seddon, The Hydrogen Bond and Crystal Engineering, *Chem. Soc. Rev.*, 1993, **22**(6), 397–407, DOI: 10.1039/cs9932200397.

47 C. B. Aakeröy, N. R. Champness and C. Janiak, Recent Advances in Crystal Engineering, *CrystEngComm*, 2010, **12**(1), 22–43, DOI: 10.1039/b919819a.

48 C. H. Hendon, A. J. Rieth, M. D. Korzyński and M. Dincă, Grand Challenges and Future Opportunities for Metal–Organic Frameworks, *ACS Cent. Sci.*, 2017, **3**(6), 554–563, DOI: 10.1021/acscentsci.7b00197.

49 M. D. Smith, E. J. Crace, A. Jaffe and H. I. Karunadasa, The Diversity of Layered Halide Perovskites, *Annu. Rev. Mater. Res.*, 2018, **48**(1), 111–136, DOI: 10.1146/annurev-matsci-070317-124406.

50 J. Yu, Q. Wang, D. O'Hare and L. Sun, Preparation of Two Dimensional Layered Double Hydroxide Nanosheets and Their Applications, *Chem. Soc. Rev.*, 2017, **46**(19), 5950–5974, DOI: 10.1039/C7CS00318H.

51 Q. Wang and D. O'Hare, Recent Advances in the Synthesis and Application of Layered Double Hydroxide (LDH) Nanosheets, *Chem. Rev.*, 2012, **112**(7), 4124–4155, DOI: 10.1021/cr200434v.

52 J. B. Lefton, W. Liu, C. McGuire, B. Lv, C. M. Brown, R. A. Klein and T. Runčevski, Synthesis, Structure and Canted Antiferromagnetism of Layered Cobalt Hydroxide Sorbate, *J. Phys. Chem. Solids*, 2023, **182**, 111568, DOI: 10.1016/j.jpcs.2023.111568.

53 R. Gieleciak, A. Hall, K. Michaelian and J. Chen, Exploring the Potential of Raman Spectroscopy for Characterizing Olefins in Olefin-Containing Streams, *Energy Fuels*, 2023, **37**(18), 13698–13709, DOI: 10.1021/acs.energyfuels.3c02014.

54 Y. Zhao, X. Luo, H. Li, J. Zhang, P. T. Araujo, C. K. Gan, J. Wu, H. Zhang, S. Y. Quek, M. S. Dresselhaus and Q. Xiong, Interlayer Breathing and Shear Modes in Few-Trilayer MoS2 and W2, *Nano Lett.*, 2013, **13**(3), 1007–1015, DOI: 10.1021/nl304169w.

55 P. E. VanNatta, C. M. Archambault, S. Wang, T. Lyu, J. D'Amelio, N. J. Martell, S. K. Watson, K. Wang, Z. Liu, M. T. Kieber-Emmons and H. Yan, High Pressure–Derived Nonsymmetrical [Cu2 O]2+ Core for Room-Temperature Methane Hydroxylation, *Sci. Adv.*, 2024, **10**(40), eadq3366, DOI: 10.1126/sciadv.adq3366.

56 H. Yan, F. Yang, D. Pan, Y. Lin, J. N. Hohman, D. Solis-Ibarra, F. H. Li, J. E. P. Dahl, R. M. K. Carlson, B. A. Tkachenko, A. A. Fokin, P. R. Schreiner, G. Galli, W. L. Mao, Z.-X. Shen and N. A. Melosh, Sterically Controlled Mechanochemistry under Hydrostatic Pressure, *Nature*, 2018, **554**(7693), 505–510, DOI: 10.1038/nature25765.

57 G. D. Saraiva, J. R. Maia, J. A. Lima, C. E. S. Nogueira, P. T. C. Freire, F. F. De Sousa, A. M. R. Teixeira and J. Mendes Filho, Pressure Induced Transformations in Sorbic Acid, *Spectrochim. Acta, Part A*, 2017, **184**, 327–334, DOI: 10.1016/j.saa.2017.05.019.

58 A. Matsumoto, K. Sada, K. Tashiro, M. Miyata, T. Tsubouchi, T. Tanaka, T. Odani, S. Nagahama, T. Tanaka, K. Inoue, S. Saragai and S. Nakamoto, Reaction Principles and Crystal Structure Design for the Topochemical Polymerization of 1,3-Dienes, *Angew. Chem., Int. Ed.*, 2002, **41**(14), 2502–2505, DOI: 10.1002/1521-3773(20020715)41:14%253C2502::AID-ANIE2502%253E3.0.CO;2-9.

59 A. Matsumoto, Polymer Structure Control Based on Crystal Engineering for Materials Design, *Polym. J.*, 2003, **35**(2), 93–121, DOI: 10.1295/polymj.35.93.

60 A. Matsumoto, S. Nagahama and T. Odani, Molecular Design and Polymer Structure Control Based on Polymer Crystal Engineering. Topochemical Polymerization of 1,3-Diene Mono- and Dicarboxylic Acid Derivatives Bearing a Naphthylmethylammonium Group as the Countercation, *J. Am. Chem. Soc.*, 2000, **122**(38), 9109–9119, DOI: 10.1021/ja001093n.

61 W. L. N. Dayaratne, R. Torres-Cadena, B. P. Schmitt, E. M. Westrick and A. Jaffe, Hybrid Bronzes: Mixed-Valence Organic–Inorganic Metal Oxides as a Tunable Material Platform, *Chem. Sci.*, 2023, **14**(39), 10756–10767, DOI: 10.1039/d3sc03828a.

62 M. N. Morey, C. M. Montone, M. R. Dworzak, G. P. A. Yap and E. D. Bloch, Tunable Synthesis of Heteroleptic Zirconium-Based Porous Coordination Cages, *Chem. Sci.*, 2025, **16**(2), 816–823, DOI: 10.1039/d4sc06023g.

63 CCDC 2526627: Experimental Crystal Structure, Determination, 2026, DOI: 10.5517/ccdc.csd.cc2qt53v.